scientific reports

Check for updates

OPEN

Optical anisotropy of pristine and reduced V_2O_5(010)

Brian Walls[1]✉, Oisín Murtagh[1], Chris M. Smith[1], Daragh Mullarkey[1], Dmitry Shulyatev[2], Karsten Fleischer[3], Ainur Zhussupbekova[1] & Igor V. Shvets[1]

The optical anisotropy of pristine and reduced single crystalline (010) orientated V_2O_5 is presented. The reduction of V_2O_5 is complex due to the abundance of V-O phases, strong dependence on the reducing conditions and multitude of reduction pathways. Different phases close in stoichiometry can exhibit drastically different electronic and optical properties. Reflectance anisotropy spectroscopy (RAS) provides a non-destructive optical probe that can be employed in real-time to monitor changes in thin films. Pristine V_2O_5(010) exhibits strong anisotropy with significant features beyond the optical bandgap of 2.5 eV. Axially resolved optical constants, extracted using ellipsometry, facilitate the calculation of the RAS which is in excellent agreement with the experimental data. Vacuum annealing has been performed at four different temperatures and X-ray Diffraction and RAS have been conducted after each anneal. Depending on the anneal temperature, different phases are introduced into the V_2O_5 crystal including V_4O_9, V_6O_{13} and VO_2. Spectral features of each of these phases are identified. V_6O_{13} is understood in terms of the axially resolved optical constants from the literature, while isotropic VO_2 modifies the total reflection once it undergoes its semiconductor-to-metal phase transition at 340 K. This understanding of the optical response of the ideal single crystal facilitates applying RAS to monitor the growth and changes of V_2O_5 thin films in real time.

Keywords Metal oxides, Vanadium oxides, Thermal oxide reduction, Reflectance anisotropy spectroscopy, Metal-to-insulator transition, Optical reflectivity, Single crystalline

Vanadium oxides are a versatile family of materials, with 4 possible oxidation states of vanadium, 2+ to 5+[1]. This leads to 4 single valence phases and a large number of mixed valence phases, each with distinct properties. For example, many vanadium oxides possess an semiconductor-to-metal transition (SMT). Each specific compound has a different magnitude of resistivity change and temperature of the SMT. V_2O_3 has a transition temperature of 168 K and a resistivity change of 10^7[2] corresponding to the largest resistivity change of the VO_x compounds, while VO_2 has a transition temperature 340 K and a resistivity change of 10^5[3]. The precise control of vanadium oxide phase and oxidation state is required to engineer a material with desired physical properties.

Current applications of vanadium oxides are industrial catalysts[4] and battery technologies[5,6] utilising V_2O_5 and advanced electronics[7,8] and sustainable window coatings utilising VO_2[9,10]. Mixed valence phases have been explored, for example V_6O_{13} in battery technologies[11]. However, their properties are not comprehensively understood, partly due to the challenge of synthesising mixed valence phases as a single crystalline product.

The initial and majority of reflectance anisotropy spectroscopy (RAS) studies have been conducted on semiconducting surfaces[12–14]; the technique has been utilised to investigate semiconductor surface reconstructions and to monitor the growth of epitaxially grown semiconductor surfaces. Furthermore, the structure of metal absorbates on metal and semiconductor surfaces or the absorbent induced reconstruction of the substrate has received considerable attention[12,15–19]. RAS represents a technique which can characterise surface and electronic structure, identify specific surface terminations and monitor changes in surface structure in real-time. Despite this, RAS studies of metal oxides have received little attention; wide-bandgap ZnO[20], superconducting cuprates[21] and more recently Fe_3O_4(110)[22,23] and $SrTiO_4$(110)[24] have been studied. The majority of these works deal with optical anisotropy originating from an anisotropic surface, due to a surface reconstruction or absorbents, on top of an isotropic bulk. RAS can probe bulk anisotropy and the vanadium oxide family is an ideal candidate for RAS measurements, with many of the crystal phases having well documented bulk structural and optical anisotropies.

[1]School of Physics and Centre for Research on Adaptive Nanostructures and Nanodevices (CRANN), Trinity College Dublin, Dublin 2, Ireland. [2]Materials Modeling and Development Laboratory, NUST MISIS, Leninskiy prosp, 4, Moscow 199049, Russia. [3]School of Physical Sciences, Dublin City University, Dublin 9, Ireland. ✉email: wallsbc@tcd.ie

Orthorhombic V_2O_5 is the vanadium oxide with the highest oxidation state and is depicted in Figure 1. It is a semiconducting material (bandgap = 2.3 eV[25,26]) and is used extensively in industry as an oxygen catalyst[4] and gas sensor[27]. The thermal reduction of single crystalline V_2O_5 at around 800 K in high vacuum[28] and oxygen[29] environments result in conversion to V_6O_{13}. In the case of the reduction of thin films Ramana *et al.*, converted amorphous V_2O_5 to V_2O_3 at 860 K[30], while Monfort *et al.* converted polycrystalline V_2O_5 to V_4O_9 at 673 K and to VO_2(B) at 773 K[31]. The reducing conditions and the nature of the V_2O_5 determines the reduction, which can be due to crystallinity, defects or both. The reduction dynamics and phase evolution as a function of reducing conditions are not well established.

To realise the applications of vanadium oxides, growth and preparation conditions need to be precisely controlled to meet requirements in material characteristics governed by structure and stoichiometry. *In-situ* non-destructive characterisation methods can provide increased control and accuracy, observing structural changes as they are induced, without exposing the sample to atmosphere. Understanding the reduction dynamics and phase evolution is vital for a fundamental physical understanding and also for the application of the vanadium oxides phases. The co-existence of several VO_x phases including mixed valance phases whose physical properties are unknown, hinders the interpretation of experiments. Identifying the reduction process and dynamics can assist greatly in the interpretation of mixed phase systems.

In this work we examine the optical anisotropy of both pristine (010) orientated V_2O_5 single crystals and crystals annealed in vacuum at various temperatures, which results in lower oxide phases in the surface region. Axially resolved ellipsometry measurements are performed and the RAS spectra is calculated from the optical constants. Vacuum annealing the V_2O_5(010) crystals at different temperatures results in different phases in the surface region and this is reflected by the drastically modified RAS spectra. A prominent feature in the infrared (IR) is assigned to V_6O_{13}(001) and the influence of VO_2 on this IR feature is revealed.

Results

RAS is a non-destructive optical probe in which linearly polarised light is at normal incidence to a sample's surface. The difference in reflectance (Δr) along two orthogonal axes of a surface plane (x, y)[32] is measured. The RAS unit ($\Delta r/r$) used is normalised to the mean reflectance (r):

$$\frac{\Delta r}{r} = 2\frac{(r_x - r_y)}{(r_x + r_y)} \tag{1}$$

where reflectances r are complex Fresnel reflection amplitudes. This measurement reveals in-plane anisotropies of the sample being analysed, and generally speaking, this is due to the anisotropic electron states or bond structures of plane normal to the light propagation direction in the region of the Fermi level[32]. Due to the measurement relying on the difference between reflections on orthogonal axes, only optically anisotropic planes give a non-zero RAS signal. In a simple two-layer model[33] (atmosphere and bulk crystal) the RAS response is related to the differences in the dielectric function as follows:

$$\frac{\Delta r}{r} = \frac{1}{\sqrt{\epsilon}}\frac{\Delta \epsilon}{\epsilon - 1} \tag{2}$$

where $\epsilon = \frac{1}{2}(\epsilon_x + \epsilon_y)$ and $\Delta\,\epsilon = \epsilon_x - \epsilon_y$. ϵ_x and ϵ_y are complex quantities.

V_2O_5 single crystals have been grown by the floating zone technique. The growth process was carried out in oxygen flow at a crystallisation rate $8\,\mathrm{mmh}^{-1}$. V_2O_5 readily cleaves along the (010) due to weak bonding in that plane[34] resulting in a reflective surface.

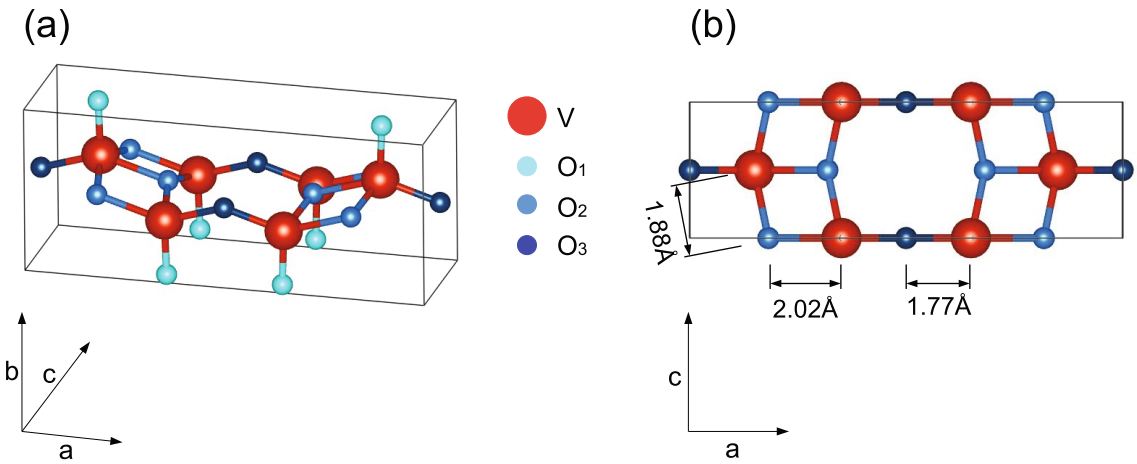

Fig. 1. (**a**) Crystal structure of orthorhombic V_2O_5 and (**b**) the (010) plane. The three oxygen atoms are distinguished. In the (010) there are V–O_2 and V–O_3 bonds, the distance of which are illustrated.

Characterisation of V_2O_5(010) single crystal

The sample surface is prepared by cleaving the single crystal in atmosphere. The θ-2θ scan in figure 2(a) reveals <010> reflexes. No reflexes due to different V_2O_5 orientation or vanadium oxide phases are observed. The RSM of the V_2O_5(010) peak [Figure 2(b)] is characteristic of a single crystal. The distribution in ω indicates there is a small angular distribution of crystallites about the surface normal. This is best visualised by the two peaks. The sharpness in 2θ indicates the crystallites are large with a consistent lattice parameter. The lattice constant (4.354Å) closely matches that of single crystalline V_2O_5[35]. The (110) lattice plane is found using an asymmetric azimuthal ϕ-scan [figure 2(c)]. It reveals a two-fold symmetry confirming the single crystallinity of orthorhombic V_2O_5.

XPS depicted in Fig. 2d confirms the single V^{5+} valence state of the crystal. The valence state of vanadium in vanadium oxides dictates the energy difference (Δ) between the O 1s and the V $2p^{3/2}$ peaks[36]. The cleaved crystal exhibits a Δ of 12.7 eV, comparable to V_2O_5(12.8 eV). For comparison, Δ for VO_2, V_2O_3 and VO are around 14.0, 14.5 and 18.0 eV, respectively[36].

RAS of the V_2O_5(010) plane

The real part of the RAS response of the V_2O_5(010) is shown in figure 3(b). The crystal is rotated in order to maximise the RAS signal, which coincide to the x and y axis in equation 1, corresponding to the [100] and [001] lattice directions, respectively. It is noted that rotating the sample only influences the magnitude of the RAS signal, an expected response from a single crystal. The real part of the RAS has sharp positive peaks at 2.9 eV, 3.5 eV and 4.4 eV, and negative peaks at 3.2 eV and 4.0 eV. Positive denotes a higher reflectivity for light polarized along the [100] axis (r_x). In the infrared (IR) region the RAS spectrum is positive and almost constant.

The real and imaginary parts of both the dielectric function and the refractive index along the [100] and [001] axes, extracted using ellipsometry measurements, are presented in Fig. 3a. Clear differences in these spectra show the optical anisotropy of the plane. The presented dielectric function is in agreement with the literature[25,37,38]. With the dielectric function and Equation 2 we calculate the real part of the RAS response (Fig. 3b). Comparison of the direct RAS measurement and calculated spectrum show good agreement. The reduced amplitude and broadening of the measured RAS is likely caused by the larger spot size and lower spectral resolution compared to the ellipsometry.

In the region from 1.3–3 eV the optical constants are well described by a Lorentzian oscillator model, which considers the induced oscillation of bound charge due to an oscillating electric field in the presence of damping[39,40]. The optical transitions are dominated by filled O 2*p* orbitals to empty V 3*d* states[41–43]. Theoretical calculations of the band structure provide insight into the anisotropy[41–43]. The bottom of the conduction band

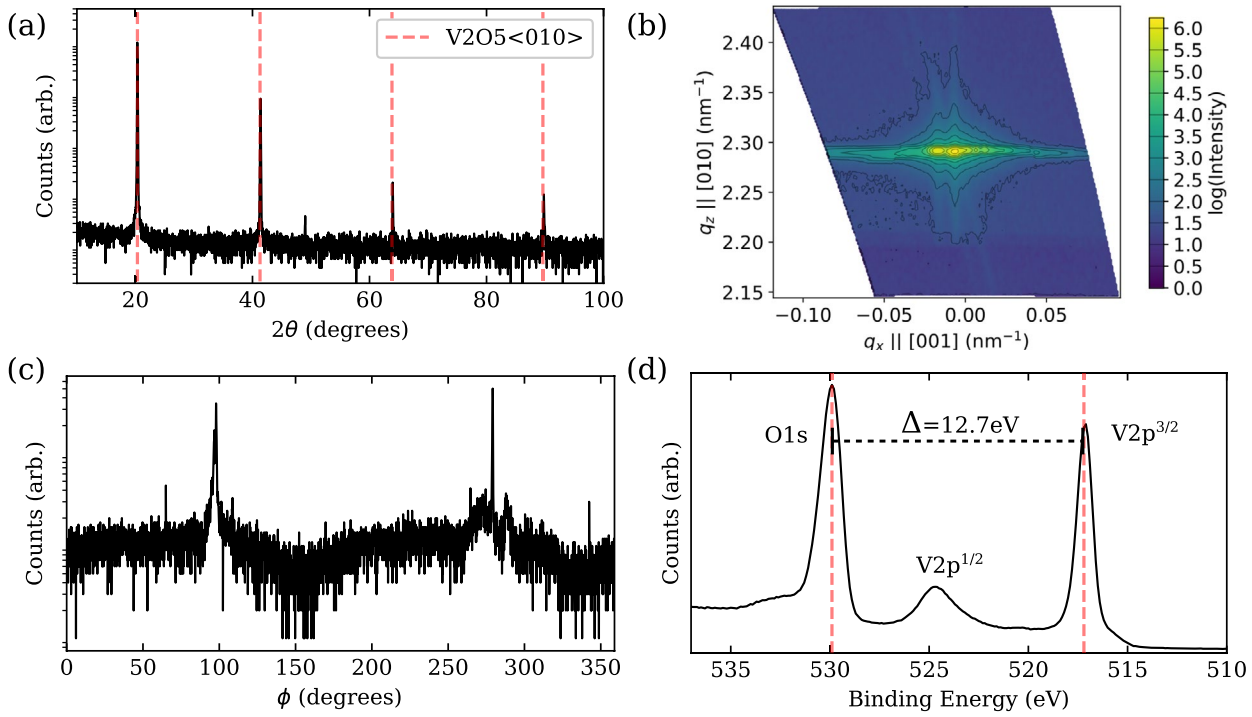

Fig. 2. Structural and chemical characterisation of the V_2O_5 single crystal. (**a**) XRD scan with <010> V_2O_5 reflexes. (**b**) RSM of the peak at 2θ = 20.3 degrees indicates a small angular distribution of crystal planes about the surface normal, characteristic of a single crystal. (**c**) Asymmetric azimuthal scan of the [110] reflex shows two fold symmetry characteristic of a single crystal in this orthorhombic system. (**d**) XPS scan of the O 1s and V 2p region (535 − 510 eV) shows the O 1s and V $2p^{3/2}$ peaks. These have a spacing (Δ) of 12.7 eV, characteristic of V^{5+}[36].

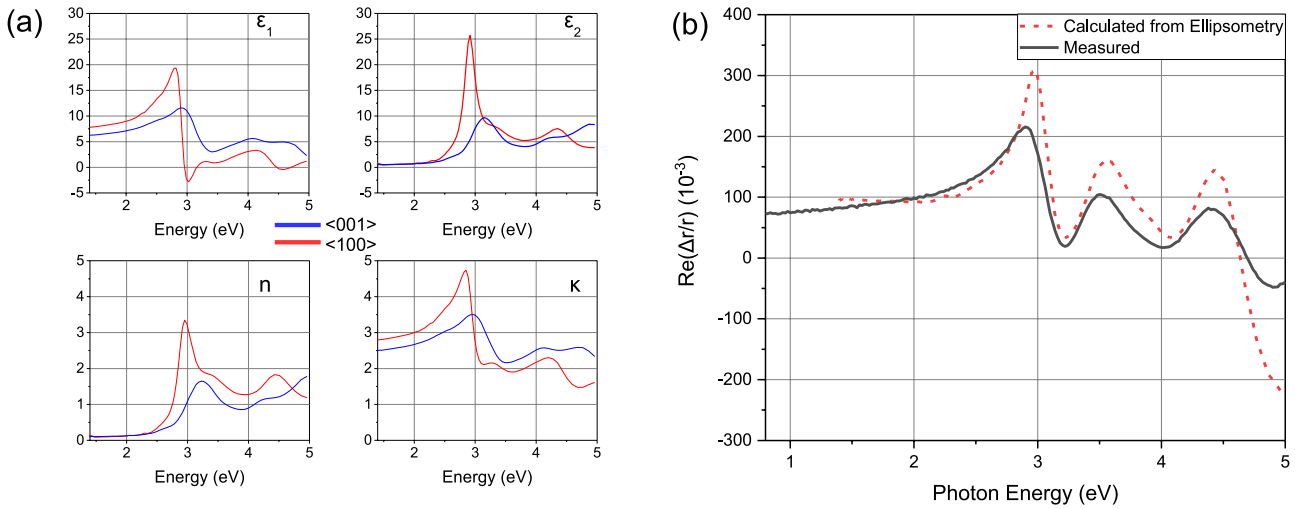

Fig. 3. (**a**) Axially resolved complex dielectric function and refractive index of the (010) plane measured via ellipsometry. (**b**) The measured dielectric function is used to calculate a RAS spectrum, and this is compared against a direct RAS measurement of the (010) plane, showing good agreement in spectral shape.

consists of two bands which are separated from several higher conduction bands by a gap in the vicinity of 0.5 eV[25,41–43]. This accounts for the peak in the optical constants in the vicinity of 3 eV beyond the indirect bandgap of 2.3 eV. The valance band maxima show considerable anisotropy. Along the [100] direction the valance band is localised while along the [001] direction exhibits a greater degree of delocalisation[25,41–43]. The localisation in the [100] accounts for the strong peak in ϵ_2 along this axis (Fig. 3a). While the more delocalised nature of the [001] direction results in a broader ϵ_2. In agreement with these calculations, Parker et al. report a sharp optical transition at 2.8 eV in the [100] direction and a broader optical transition at 3.2 eV in the [001] direction[25]. The anisotropic absorption lines is linked to the oxygen structure in the [010] plane[41–43], which is depicted in Fig. 1. The V-O bonds vary from 1.60–2.02 Å[25,35,41]. The spatial carrier densities and the correlated optical transitions strongly depend on the V-O distance, as has been revealed by density functional theory calculations[41]. Bonds along the [100] axis are V–O(2) coordinated bonds, possessing a length of 1.78 Å, and longer V–O(3) bonds, with length 2.02 Å. Along the [001] axis, there are only V–O(3) bonds with length 1.88 Å.

Annealed V_2O_5 crystals

The four V_2O_5 crystals were annealed at difference temperatures in a pressure of 5×10^{-5} mbar. The evolution of the RAS is summarised in this section. The stated anneal time is the cumulative time of annealing at that temperature. Prior to discussing the results, the reduction pathways of V_2O_5 are discussed, which motivates our interpretation of the data. The Wadsley phases of the vanadium-oxygen system (V_nO_{2n+1}) range from V_2O_5(n = 2) to VO_2(B) (n = ∞). Other Wadsley phases, relevant to our discussion, are V_6O_{13} and V_4O_9. V_2O_5 is orthorhombic and consists of a V_2O_3-O_2 stacking sequence along its [010] direction. Orthorhombic V_4O_9 consists of a V_2O_3-O_2-V_2O_3-O stacking sequence along its [001] direction[44] and is based on a super-lattice of oxygen vacancies within V_2O_5 residing in the oxygen layers[45]. Reports of V_4O_9 are scarce; it is synthesised via the reduction of V_2O_5[31,44–46] with V_4O_9[001] aligned with V_2O_5[010][31,44,45]. Along its [001] direction V_6O_{13} consists of a V_2O_3-O_2-V_2O_3-V_2O_3-O_2 stacking sequence. V_6O_{13} can be formed from V_2O_5 via the removal of every third O_2 plane. This reduction and a shear operation produces monoclinic V_6O_{13} from orthorhombic V_2O_5 with V_6O_{13}[001] aligned with V_2O_5[010][28]. Similarly to V_2O_5 and V_6O_{13}, VO_2(B) consists of V_2O_3 and O_2 planes. The stacking sequence is V_2O_3-V_2O_3-O_2. This corresponds to removing every second O_2 plane of V_2O_5. This combined with a shear operation can produce monoclinic VO_2(B). This results in VO_2(B)[001] aligned with V_2O_5[010]. It is clear that V_4O_9(V_2O_3-**O**-V_2O_3-O_2) can act as a seed for the formation of VO_2(B) (V_2O_3-V_2O_3-O_2), in agreement with the literature[31]. Based on these discussed reduction mechanisms, in the following analysis of the XRD spectra V_2O_5<010>, V_4O_9<001>, V_6O_{13}<001> and VO_2(B)<001> reflexes are considered. The only exception is V_6O_{13}<010>, which has been observed by Transmission Electron Microscopy (TEM)[47].

Starting with the crystal annealed at 600 K, the RAS signal (Fig. 4a) of the 20 min anneal (black) produces noticeable changes to the pristine (Fig. 3b) spectra with peaks now at negative RAS units at energies greater than 3 eV. However, there is resemblence to the pristine spectra from the IR to around 3.2 eV. Further annealing reduces the optical anisotropy. The spectra after 4 (blue) and 6 hours (green) are qualitatively the same characterised by a minimum-maximum at $2.7 - 3.1$ eV and a small positive peak at 3.5 eV. At all stages of the annealing, XRD reveals V_4O_9<001> and V_2O_5<010> reflexes.

At 700 K, the initial 20 min anneal (black) produces a RAS signal that exhibits a minimum-maximum at $2.7 - 3.1$ eV and a small positive peak at 3.5 eV [Figure 4(b)]. The XRD of the 20 min 700 K anneal shows a strong V_4O_9 peak, with small peaks assigned to V_6O_{13}(001). Additional annealing results in V_6O_{13}(001) increasing in intensity in the XRD. VO_2(B)<001> is assigned tentatively. At the same time the RAS spectra

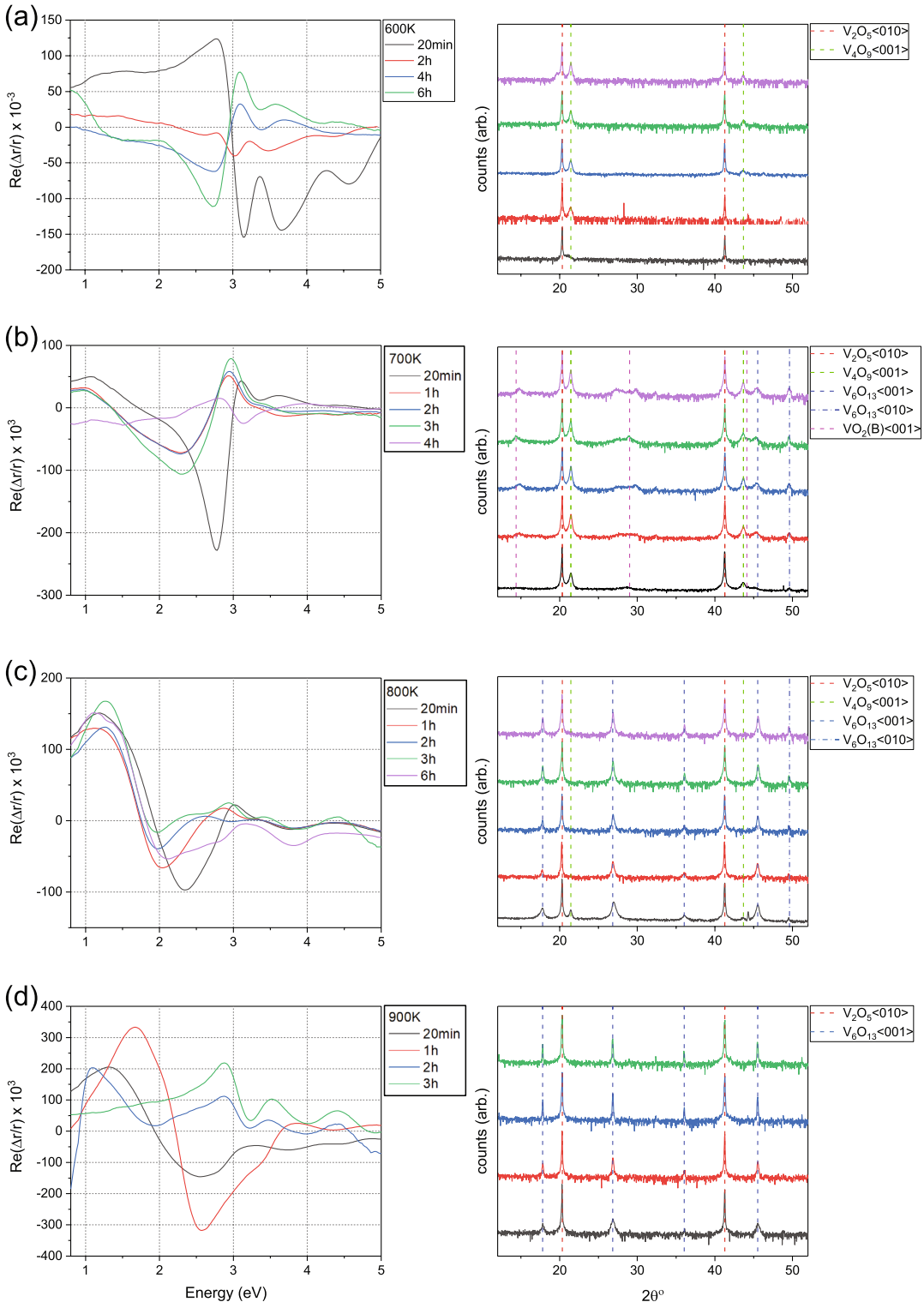

Fig. 4. RAS and XRD of V_2O_5 crystals annealed at 600, 700, 800 and 900 K in (**a**–**d**). (**a**) 600 K; Significant changes in the RAS induced by the initial 20 minute anneal. Minima-maxima structure (2.7–3.1 eV) in 4 and 6 h spectra. Optical anisotropy is reduced with additional annealing. XRD is characterised by V_2O_5<010> and V_4O_9<001>. (**b**) 700 K; Initial 20 min anneal induces a sharp negative structure at 2.8 eV. Cumulative anneals of 1, 2 and 3 h characterised by minima-maxima structure (2.3–2.9 eV). Additional annealing reduce the optical anisotropy. XRD characterised by strong V_2O_5<010> and V_4O_9<001> and comparatively weak V_6O_{13}<001>. (**c**) 800 K; Strong IR structure in all spectra. XRD dominated by V_2O_5<010> and V_6O_{13}<001>. V_4O_9<001> only observed for the initial 20 minute anneal. (**d**) 900 K; Considerable positive IR structure and negative structure around 2.5 eV. Spectra is V_2O_5<010>-like after 2 and 3 h of cumulative annealing. XRD dominated by V_2O_5<010> and V_6O_{13}<001>.

changes, with the minima-maxima shifting the lower energy and the minima becoming broader and lower in magnitude. After 4 h (purple) the optical anisotropy is reduced.

At 800 K the initial 20 min anneal produces a RAS signal (black) that is characterised by a strong IR response and a broad minimum at 2.3 eV (Fig. 4). Turning to the XRD the 20 min anneal results in only V_6O_{13} peaks indicating the IR response is due to this phase. We note this is the first XRD is characterised entirely by V_6O_{13} and the first observation of the IR structure in the RAS. Further annealing shifts the broad RAS minima from 2.5 to 2 eV progressively and to lower magnitude. At the same time the positive IR response is enhanced. The XRD is characterised by V_6O_{13} and V_2O_5 at further annealing steps. VO_2 is present in the crystal after 2 h of annealing and longer. The presence is VO_2 is determined by resistance-temperature measurements presented in the Supplemental Information. At around 343 K the resistance of VO_2 change by several orders of magnitude. VO_2 is not observed in crystal annealed at the other temperatures. The influence of VO_2 is discussed below.

At 900 K the initial 20 min anneal (red) produces a strong RAS response in the IR with a positive broad feature but also broad negative structures at higher energies with the most prominent being at 2.5 eV(Fig. 4d). A further anneal (1 h) enhances both the positive structure in the IR and the negative structure at 2.5 eV. The IR structure is shifted to higher energy. Further annealing (blue) modifies the IR structure but at higher energies the spectra is very similar to the V_2O_5(010) spectra. A further hour anneal (green) reverts the spectra back to the original V_2O_5 with very little deviation. The XRD at this temperature is straight forward being dominated by V_6O_{13}(001) (Fig. 4). Clearly the RAS is sensitive to more than XRD as the spectra changes with each annealing step. The spectra becoming V_2O_5(010)-like—even when V_6O_{13}(001) is present in the surface region—indicates that the V_6O_{13} is no longer contributing to the RAS signal. This is suggested to be due to a reduction in symmetry; if the (001)-orientated V_6O_{13} is polycrystalline in-plane, it will not produce a net RAS response. Evidently the surface region is less ordered. The V_2O_5 signal is from the underlying non-reduced bulk.

In Fig. 5 we compare spectra of crystals annealed at different temperatures. The initial 20 min anneal at 700 K is qualitatively similar to 600 K after 4 and 6 h (Fig. 5a). Each spectra contains a minimum-maximum at $2.4 - 2.6$ eV and a small positive peak at 3.5 eV. The XRD of each of these crystals is characterised entirely by V_4O_9<001> and V_2O_5<010> (Fig. 5b). Therefore, we attribute the minima-maxima feature from $2.5 - 3.5$ eV to V_4O_9. Note, the a-axis of V_4O_9 and V_2O_5 are aligned[48]. Similar to V_2O_5, let's consider V-O distance in the V_4O_9(001) plane. If one assumes the electronic structure of V_4O_9 is similar to V_2O_5, the optical transitions are dominated by oxygen (valence band) to vanadium (conduction band) and the energy of the optical transitions is inversely proportional to the V-O distance. The smallest V-O distance of 1.68 Å is along V_4O_9[010] (y-axis in Eq. 1), while along V_4O_9[100] (x-axis in Eq. 1) the V–O distance is 1.78 Å. This is opposite to V_2O_5 where the shortest V-O bond is in the x-axis. Within this simple framework of V-O bond distance for V_4O_9(001) we can hypothesise a negative RAS peak at lower energies followed by a positive peak, as is observed. An understanding of the electronic and optical properties of V_4O_9 is required to comprehensively discuss the contributions from this phase, which has received very little attention.

V_6O_{13} IR structure

As was discussed above, with increasing temperature (or duration of the anneal in the case of 700 K) a large IR feature develops. This directly coincides with the emergence of V_6O_{13}(001) peaks in the XRD. A RAS feature from V_6O_{13}(001) at low energy is unsurprising as the (001) plane is anisotropic and V_6O_{13} is metallic. In this section on the basis of V_6O_{13} ellipsometry measurements from the literature we confirm that this IR structure is due to anisotropic V_6O_{13}(001).

It is well established that the epitaxial reduction of V_2O_5(010) gives rise to the formation of V_6O_{13}(001) with their [100] axes aligned[28,47]. In Figure 6 we depict two RAS spectra which exhibit a strong IR RAS response. The corresponding XRD reveals these two samples are dominated by V_6O_{13}(001) and V_2O_5(010). Van Hove *et al.* measured the 45° incidence reflection and absorption spectrum of V_6O_{13} along the [100] and [010]

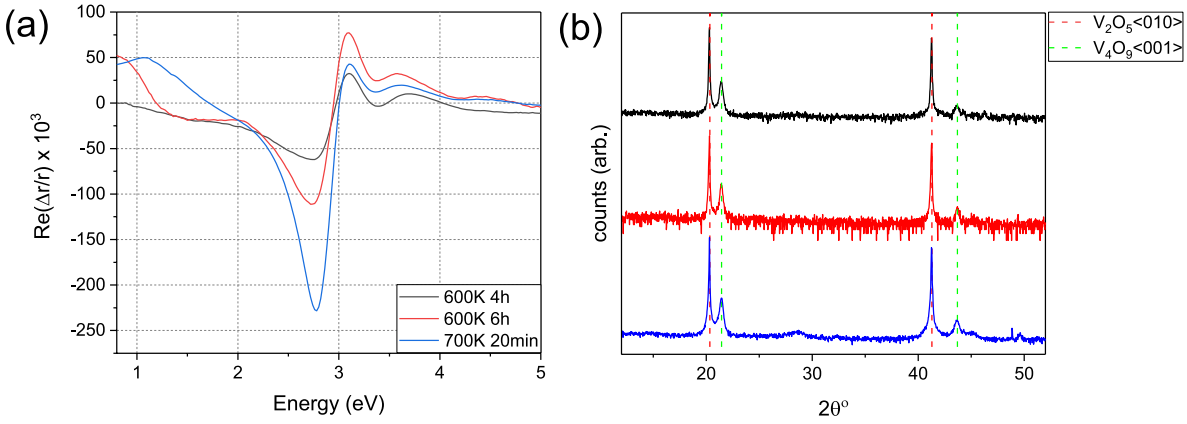

Fig. 5. (**a**) Comparison between RAS spectra of crystal annealed at different temperatures. A minima-maxima structure at 2.8–3.1eV is observed for the crystal annealed for a considerable duration (4 and 6 h depicted) at 600 K and for the crystal annealed for a short duration (20 minutes) at a higher temperature of 700 K. (**b**) Corresponding XRD characterised by V_2O_5<010> and V_4O_9<001>.

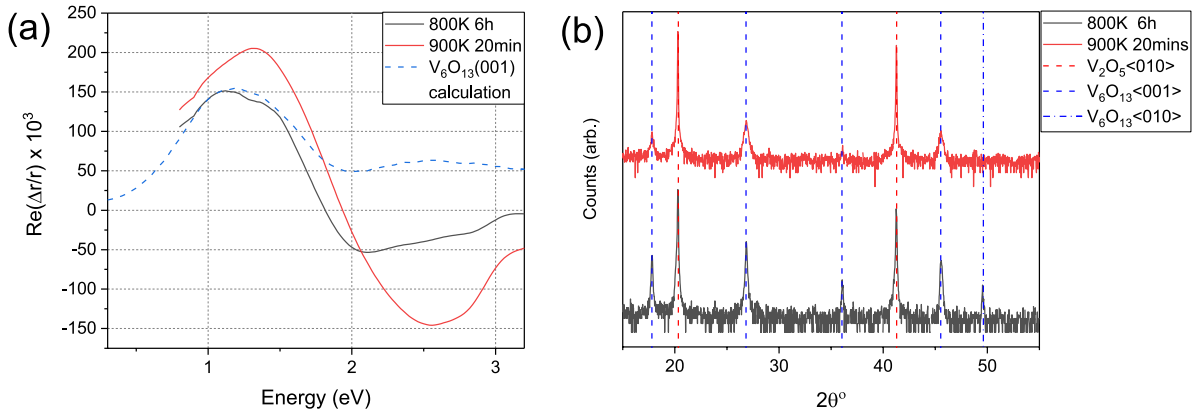

Fig. 6. (**a**) The calculated (001) RAS spectrum of V_6O_{13} compared to the measured RAS spectrum of two single crystal samples annealed at different times and temperatures. This positive feature between $1-2$ eV is identified as a V_6O_{13} feature. (**b**) XRD pattern of the two annealed samples showing V_6O_{13}(001) reflections.

directions in the range $0.2-3.2$ eV[49]. These values are converted to a complex dielectric function and using Equation 2 a RAS spectrum for the V_6O_{13}(001) plane is generated (Fig. 6a). This spectrum has a maximum at 1.2 eV and a minimum at 2 eV, matching the features seen in the presented experimental spectra. V_2O_5(010) exhibits a constant RAS in this region, and therefore will only offset this feature. Based on these findings we conclude this IR feature seen in our samples is due to V_6O_{13}(001).

Van Hove et al. attribute the absorption features below 2.2 eV to inter-band transitions in the partially filled V3*d* band[49]. Anisotropies in charge state and geometry are present, but it is difficult to specifically attribute increased reflectivity in the [100] direction compared to [010] due to V-V structures. DFT electron-structure calculations[50] suggest that t_{2g} transitions will dominate the IR, V $3d_{xz}$ t_{2g} shows strong anisotropy with the [100] direction exhibiting flat bands around the Fermi level and ~ 1 eV above. [010] on the other hand shows significant dispersion. The presented positive RAS feature corresponds to a high reflectivity along the V_6O_{13} [100] direction in comparison to V_6O_{13}[010].

RAS measurements across the VO_2 MIT

VO_2 undergoes a SMT at 340 K[3]. Below the transition temperature, the structure is monoclinic and semiconducting, while above it becomes rutile (orthorhombic) and metallic. Moving through the transition from the rutile phase, vanadium ions form dimer pairs along the rutile [001] lattice direction creating the monoclinic structure. The shift of ions causes crystal field splitting of the V-O orbitals resulting in a bandgap opening[51].

VO_2 has been reported to form with a polycrystalline structure through reduction[52], so we do not expect an epitaxial relationship between VO_2 and V_2O_5. Furthermore, members of the Wadsley (V_nO_{2n+1}) series cannot be related to Magneli (V_nO_{2n-1}) phases by a common substructure. This is emphasised by the complex transformation of VO_2(B) (Wadsley) to VO_2(Magneli); it involves an initial disordering step followed by a reordering into VO_2[53]. In our recent work[47], an V_2O_5 crystal annealed at 800 K in high vacuum was examined by reciprocal space mapping. VO_2 was observed in the reduced crystal and was polycrystalline within the probed angular window. Therefore, VO_2 will not generate a RAS signal. A clear recorded change in optical properties of VO_2 over the transition is an increase in absorption in the $0-1$ eV region[54,55]. Therefore, the SMT transition can modify the RAS spectra by modifying the total reflectance.

In order to establish VO_2's influence on the RAS spectra we have examined a reduced crystal below and above the VO_2 SMT temperature. This crystal have been annealed for 6 h at 800 K and XRD and resistance measurements indicate it contains VO_2.

Figure 7, shows the previously established V_6O_{13} feature with a maximum at 1.2 eV as the sample is heated through 340 K. The cooling cycle is not not depicted here for the sake of clarity. The RAS signal decreases in the range $0.8-1.5$ eV as the temperature increases, while no change is seen in the $1.5-2$ eV region. The decrease in signal is attributed to the increased absorption, and hence reflectivity, of the metallic VO_2 phase in the IR[54,55]. Figure 7 (inset) plots the RAS signal at 0.8 eV as a function of temperature for both heating and cooling. The resulting hysteric plot is characteristic of the VO_2 first order transition. The increased reflectivity of VO_2 across the transition temperature results in a decreasing RAS as has been observed in temperature dependant Fe_3O_4 measurements[22].

Conclusions

The optical anisotropy of pristine single crystalline and vacuum annealed V_2O_5 has been examined ex-situ by reflectance anisotropy spectroscopy (RAS) in the range of 0.8–5 eV. The RAS spectra of the (010) plane of V_2O_5 exhibits a constant signal in the IR range and significant structure beyond 2.5 eV. Axially resolved ellipsometry measurements facilitate the calculation of the RAS spectra, which is in good agreement.

The vacuum annealing of the single crystal V_2O_5(010) results in significant changes in the RAS spectra. The changes are characterised by the introduction of additional lower oxide phases, as confirmed by XRD

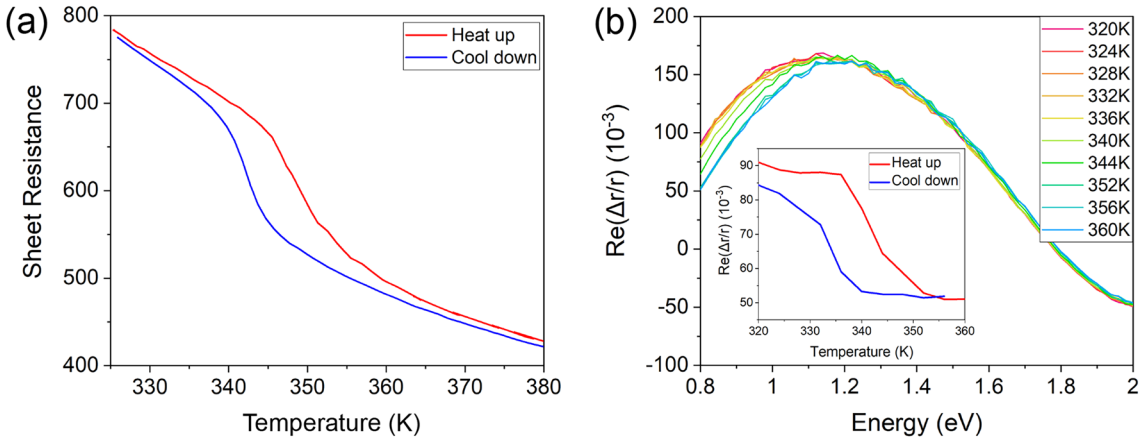

Fig. 7. (**a**) Sheet resistance vs temperature and (**b**) change in the V_6O_{13} RAS feature as the temperature moves through the VO_2 MIT temperature (340 K). The inset graph shows the measured RAS signal at 0.8 eV through heating and cooling cycles. The shape of this graph is characteristic of the VO_2 MIT transition.

measurements performed after each anneal. The RAS spectra are dependant on the annealing temperature due to the reduction of V_2O_5 being strongly dependant on the temperature of vacuum annealing. However, RAS is far more sensitive to these structural and chemical changes than XRD, with significant optical modification observed while the diffraction pattern is unchanged.

Spectral signatures of V_4O_9, V_6O_{13} and VO_2 are identified. The IR signal of V_6O_{13} is calculated via the optical constants from the literature and shows good agreement with our RAS measurements. While VO_2 does not possess an optically anisotropic response, it's reflectance in the IR increases as it is heated through the SMT and becomes metallic at around 340 K. This changes the IR RAS magnitude, which is normalised by the total reflectance. The V_4O_9 response is assigned based on the comparison to XRD measurements. There are no reports of the optical constants of this phase.

RAS can be employed in-situ as a non-destructive probe to identify changes in the stoichiometry and crystal structure in real-time. This ex-situ study demonstrates the sensitivity of RAS to these changes and identifies spectral signatures of multiple phases in this system.

Methods

RAS spectra were recorded at near-normal incidence with an in-house built reflectance anisotropy spectrometer which follows the Aspnes design[56]. Light from a Xe lamp passes through a Rochon Mg_2F polariser and is reflected from the sample. The beam passes through a photoelastic modulator (PEM), an analyzing polariser, and a monochromator before finally reaching a diode detector system. All measurements were performed from 0.8 to 5.5 eV; the broad spectral range has been realized using a monochromator and two individual photo diodes (InGaAs, Si). The real component of the complex RAS is presented.

V_2O_5 single crystals have been grown by the floating zone technique. The growth process was carried out in oxygen flow at a crystallisation rate $8\,mmh^{-1}$. V_2O_5 readily cleaves along the (010) due to weak bonding in that plane[34] resulting in a reflective surface.

XRD characterisation utilized a Bruker D8 Discover, with a monochromatic copper Kα1 source and a position-sensitive detector (LynxEye), also used for reciprocal space maps (RSM). Spectroscopic ellispometry of a pristine V_2O_5 crystal was performed using the variable angle spectroscopic ellispometry (VASE) method on a Sopra GESP 5 spectroscopic ellipsometer, which uses a rotating polariser configuration. RT measurements were performed using a linear four-point probe on a heated stage. Temperatures were restricted to room temperature and above. XPS measurements of the pristine crystal were performed using an Omicron Multi-Probe XPS system using monochromated Al Kα X-rays (XM 1000, 1486.7 eV) with an instrumental resolution of 0.6 eV. Spectra have been analysed and fitted with CasaXPS. Temperature dependent RAS measurements were performed using a PID controlled heater for above room temperature measurements.

Data availability

Raw data can be made available upon request to the corresponding author.

Received: 6 March 2025; Accepted: 16 June 2025
Published online: 01 July 2025

References

1. Wells, A. F. *Structural Inorganic Chemistry* (Oxford University Press, 2012).
2. Adler, D., Feinleib, J., Brooks, H. & Paul, W. Semiconductor-to-metal transitions in transition-metal compounds. *Phys. Rev.* **155**, 851 (1967).
3. Zylbersztejn, A. & Mott, N. F. Metal-insulator transition in vanadium dioxide. *Phys. Rev. B* **11**, 4383 (1975).

4. Louie, D. K. *Handbook of Sulphuric Acid Manufacturing* (DKL Engineering, Inc., 2005).
5. Chao, D. et al. A V_2O_5 conductive-polymer core-shell nanobelt array on three-dimensional graphite foam: a high-rate, ultrastable, and freestanding cathode for lithium-ion batteries. *Adv. Mater.* **26**, 5794–5800 (2014).
6. Wang, Y., Takahashi, K., Lee, K. H. & Cao, G. Nanostructured vanadium oxide electrodes for enhanced lithium-ion intercalation. *Adv. Funct. Mater.* **16**, 1133–1144 (2006).
7. Zhou, Y. & Ramanathan, S. Mott memory and neuromorphic devices. *Proc. IEEE* **103**, 1289–1310 (2015).
8. Yang, Z., Ko, C. & Ramanathan, S. Oxide electronics utilizing ultrafast metal-insulator transitions. *Annu. Rev. Mater. Res.* **41**, 337–367 (2011).
9. Cui, Y. et al. Thermochromic VO_2 for energy-efficient smart windows. *Joule* **2**, 1707–1746 (2018).
10. Ye, H. & Long, L. Smart or not? A theoretical discussion on the smart regulation capacity of vanadium dioxide glazing. *Solar Energy Mater. Solar Cells* **120**, 669–674 (2014).
11. Shan, L. et al. Highly reversible phase transition endows V_6O_{13} with enhanced performance as aqueous zinc-ion battery cathode. *Energy Technol.* **7**, 1900022. https://doi.org/10.1002/ente.201900022 (2019).
12. Weightman, P., Martin, D. S., Cole, R. J. & Farrell, T. Reflection anisotropy spectroscopy. *Rep. Prog. Phys.* **68**, 1251 (2005).
13. Zettler, J.-T. Characterization of epitaxial semiconductor growth by reflectance anisotropy spectroscopy and ellipsometry. *Prog. Crystal Growth Character. Mater.* **35**, 27–98 (1997).
14. Kamiya, I., Aspnes, D. E., Florez, L. T. & Harbison, J. P. Reflectance-difference spectroscopy of (001) GaAs surfaces in ultrahigh vacuum. *Phys. Rev. B* **46**, 15894 (1992).
15. Chan, T.-L. et al. First-principles studies of structures and stabilities of Pb/Si(111). *Phys. Rev. B* **68**, 045410 (2003).
16. Power, J. R. et al. Sb-induced (1×1) reconstruction on Si(001). *Phys. Rev. B* **67**, 115315 (2003).
17. Astropekakis, A. et al. Influence of Sn on the optical anisotropy of single-domain Si(001). *Phys. Rev. B* **63**, 085317 (2001).
18. Martin, D. S., Davarpanah, A. M., Barrett, S. D. & Weightman, P. Reflection anisotropy spectroscopy of the Na/Cu(110) (1×2) surface reconstruction. *Phys. Rev. B* **62**, 15417 (2000).
19. Fleischer, K., Chandola, S., Esser, N., Richter, W. & McGilp, J. F. Reflectance anisotropy spectroscopy of Si (111)-(4×1)-In. *Phys. Status Solidi (a)* **188**, 1411–1416 (2001).
20. Rossow, U., Goldhahn, R., Fuhrmann, D. & Hangleiter, A. Reflectance difference spectroscopy RDS/RAS combined with spectroscopic ellipsometry for a quantitative analysis of optically anisotropic materials. *Phys. Status Solidi (b)* **242**, 2617–2626 (2005).
21. Bahrs, S. et al. Effect of light on the reflectance anisotropy and chain-oxygen related Raman signal in untwinned, underdoped crystals of $YBa_2Cu_3O_{7-\delta}$. *J. Phys. Chem. Solids* **67**, 340–343 (2006).
22. Fleischer, K. et al. Reflectance anisotropy spectroscopy of magnetite (110) surfaces. *Phys. Rev. B* **89**, 195118 (2014).
23. Walls, B. et al. Reflectance anisotropy spectroscopy of Fe_3O_4(110): Anisotropic strain. *Phys. Rev. B* **98** (2018).
24. Fleischer, K., Kim, S., Walls, B., Zhussupbekov, K. & Shvets, I. V. Optical anisotropy of $SrTiO_3$(110) for different surface terminations. *Phys. Status Solidi (B)* **255**, 1700459. https://doi.org/10.1002/pssb.201700459 (2017).
25. Parker, J., Lam, D., Xu, Y.-N. & Ching, W. Optical properties of vanadium pentoxide determined from ellipsometry and band-structure calculations. *Phys. Rev. B* **42**, 5289 (1990).
26. Lambrecht, W., Djafari-Rouhani, B. & Vennik, J. On the origin of the split-off conduction bands in V_2O_5. *J. Phys. C Solid State Phys.* **14**, 4785 (1981).
27. Alrammouz, R. et al. V_2O_5 gas sensors: A review. *Sens. Actuators A Phys.* **332**, 113179. https://doi.org/10.1016/j.sna.2021.113179 (2021).
28. Colpaert, M. N., Clauws, P., Fiermans, L. & Vennik, J. Thermal and low energy electron bombardment induced oxygen loss of V_2O_3 single crystals: Transition into V_6O_{13}. *Surf. Sci.* **36**, 513–525. https://doi.org/10.1016/0039-6028(73)90399-3 (1973).
29. Devriendt, K., Poelman, H. & Fiermans, L. Thermal reduction of vanadium pentoxide: An XPD study. *Surf. Sci.* **433–435**, 734–739. https://doi.org/10.1016/s0039-6028(99)00171-5 (1999).
30. Ramana, C. V., Utsunomiya, S., Ewing, R. C. & Becker, U. Formation of V_2O_3 nanocrystals by thermal reduction of V_2O_5 thin films. *Solid State Commun.* **137**, 645–649. https://doi.org/10.1016/j.ssc.2006.01.026 (2006).
31. Monfort, O. et al. Reduction of V_2O_5 thin films deposited by aqueous sol–gel method to VO_2(b) and investigation of its photocatalytic activity. *Appl. Surf. Sci.* **322**, 21–27. https://doi.org/10.1016/j.apsusc.2014.10.009 (2014).
32. Weightman, P., Martin, D., Cole, R. & Farrell, T. Reflection anisotropy spectroscopy. *Rep. Prog. Phys.* **68**, 1251 (2005).
33. Aspnes, D. Analysis of modulation spectra of stratified media. *JOSA* **63**, 1380–1390 (1973).
34. Haber, J., Witko, M. & Tokarz, R. Vanadium pentoxide I. Structures and properties. *Appl. Catal. A Gen.* **157**, 3–22 (1997).
35. Enjalbert, R. & Galy, J. A refinement of the structure of V_2O_5. *Acta Crystallogr. Sect. C Cryst. Struct. Commun.* **42**, 1467–1469 (1986).
36. Hryha, E., Rutqvist, E. & Nyborg, L. Stoichiometric vanadium oxides studied by XPS. *Surf. Interface Anal.* **44**, 1022–1025 (2012).
37. Mokerov, V., Makarov, V., Tulvinskii, V. & Begishev, A. Optical properties of vanadium pentoxide in the region of photon energies from 2 eV to 14 eV. *Opt. Spectrosc.(USSR) (Engl. Transl.) (United States)* **40** (1976).
38. Lamsal, C. & Ravindra, N. Optical properties of vanadium oxides—An analysis. *J. Mater. Sci.* **48**, 6341–6351 (2013).
39. Lorentz, H. A. *The Theory of Electrons and Its Applications to the Phenomena of Light and Radiant Heat*. Vol. 29 (GE Stechert & Company, 1916).
40. Stenzel, O. *Linear Optical Constants II: Classical Dispersion Models*. 359–380 (Springer, 2022).
41. Nguyen, T. D. H., Vo, K. D., Pham, H. D., Huynh, T. M. D. & Lin, M.-F. Electronic and optical excitation properties of vanadium pentoxide V_2O_5. *Comput. Mater. Sci.* **198**, 110675. https://doi.org/10.1016/j.commatsci.2021.110675 (2021).
42. Chakrabarti, A. et al. Geometric and electronic structure of vanadium pentoxide: A density functional bulk and surface study. *Phys. Rev. B* **59**, 10583–10590. https://doi.org/10.1103/physrevb.59.10583 (1999).
43. Eyert, V. & Höck, K.-H. Electronic structure of V_2O_5. *Phys. Rev. B* **57**, 12727–12737. https://doi.org/10.1103/physrevb.57.12727 (1998).
44. Yamazaki, S. et al. Synthesis, structure and magnetic properties of V_4O_9—A missing link in binary vanadium oxides. *J. Solid State Chem.* **183**, 1496–1503. https://doi.org/10.1016/j.jssc.2010.04.007 (2010).
45. Grymonprez, G., Fiermans, L. & Venink, J. Structural properties of vanadium oxides. *Acta Crystallogr. Sect. A* **33**, 834–837. https://doi.org/10.1107/s0567739477002010 (1977).
46. Tilley, R. & Hyde, B. An electron microscopic investigation of the decomposition of V_2O_5. *J. Phys. Chem. Solids* **31**, 1613–1619. https://doi.org/10.1016/0022-3697(70)90045-4 (1970).
47. Walls, B. et al. VO_x phase mixture of reduced single crystalline V_2O_5: VO_2 resistive switching. *Materials* **15**, 7652. https://doi.org/10.3390/ma15217652 (2022).
48. Yamazaki, S. et al. Synthesis, structure and magnetic properties of V_4O_9—A missing link in binary vanadium oxides. *J. Solid State Chem.* **183**, 1496–1503 (2010).
49. Van Hove, W., Clauws, P. & Vennik, J. Optical properties of V_6O_{13} single crystals in the metallic and the semiconducting phase. *Solid State Commun.* **33**, 11–16 (1980).
50. Toriyama, T., Nakayama, T., Konishi, T. & Ohta, Y. Charge and orbital orderings associated with metal-insulator transition in V_6O_{13}. *Phys. Rev. B* **90**, 085131. https://doi.org/10.1103/physrevb.90.085131 (2014).
51. Goodenough, J. B. The two components of the crystallographic transition in VO_2. *J. Solid State Chem.* **3**, 490–500 (1971).

52. Leroux, C., Nihoul, G. & Van Tendeloo, G. From VO_2(B) to VO_2(R): Theoretical structures of VO_2 polymorphs and in situ electron microscopy. *Phys. Rev. B* **57**, 5111 (1998).
53. Valmalette, J.-C. & Gavarri, J.-R. High efficiency thermochromic VO_2(R) resulting from the irreversible transformation of VO_2(B). *Mater. Sci. Eng. B* **54**, 168–173 (1998).
54. Chain, E. E. Optical properties of vanadium dioxide and vanadium pentoxide thin films. *Appl. Opt.* **30**, 2782–2787 (1991).
55. Verleur, H. W., Barker Jr, A. & Berglund, C. Optical properties of VO_2 between 0.25 and 5 eV. *Phys. Rev.* **172**, 788 (1968).
56. Aspnes, D. & Studna, A. Anisotropies in the above—Band-gap optical spectra of cubic semiconductors. *Phys. Rev. Lett.* **54**, 1956 (1985).

Acknowledgements

The authors would like to acknowledge Research Ireland under grant number 22/FFP-A/10353, an IRC Award (GOIPD/2022/443) and Erasmus Plus mobility grants (2017-1-IE02-KA107-000538, 2018-1-IE02-KA107-000589 and 2019-1-IE02-KA107-000642).

Author contributions

B.W. conceived the experiment. O.M. and B.W. conducted the RAS measurements. O.M conducted variable temperature RAS measurements. C.M.S. conducted the ellipsometry measurements. D.M. and O.M. conducted asymmetric XRD measurements. O.M. conducted the symmetric RAS measurements. A.Z. conducted the XPS measurements. D.S. grew the samples. K.F. calculated the RAS spectra from the ellipsometry data. B.W., O.M., K.F., and I.V.S. discussed and analyzed the results. B.W. and O.M. wrote the manuscript. All Authors reviewed the manuscript.

Declarations

Competing interests

The authors declare no competing interests.

Additional information

Supplementary Information The online version contains supplementary material available at https://doi.org/10.1038/s41598-025-07519-z.

Correspondence and requests for materials should be addressed to B.W.